Available online at www.sciencedirect.com
ScienceDirect
Journal of the European Ceramic Society 31 (2011) 2497–2503
www.elsevier.com/locate/jeurceramsoc

# Processing of highly oriented (K,Na)$NbO_3$ thin films using a tailored metal-alkoxide precursor solution

Yoshifumi Nakashima, Wataru Sakamoto *, Toshinobu Yogo

*Division of Nanomaterials Science, EcoTopia Science Institute, Nagoya University, Furo-cho, Chikusa-ku, Nagoya 464-8603, Japan*

Available online 17 May 2011

**Abstract**

Highly oriented lead-free $K_{0.5}Na_{0.5}NbO_3$ (KNN) thin films were synthesized by chemical solution deposition. The analysis of the KNN precursor solution revealed that the KNN precursor consists of complex metal alkoxides of potassium and sodium hexaalkoxy niobates with highly symmetric Nb-O octahedra. KNN precursor films were crystallized in a perovskite phase with a (1 0 0) preferred orientation on Pt(1 0 0)/MgO(1 0 0) substrates at 650 °C. The three-dimensional relationship between KNN(1 0 0) and Pt(1 0 0)/MgO(1 0 0) is confirmed by the fourfold symmetry of the pole figure. The fourfold symmetry indicates that the synthesized films are oriented in both the c and a, b directions on the Pt(1 0 0) surface. Although the insulating resistance was not sufficiently high at room temperature, the (1 0 0)-oriented KNN thin films showed potentially larger polarizations compared to the KNN thin films with no preferred orientation at low temperatures. The $2P_r$ and $2E_c$ of the oriented KNN films at −190 °C were 41.0 μC/cm$^2$ and 90 kV/cm, respectively.


*Keywords:* Sol–gel processes; Ferroelectric properties; Perovskites; Niobates; Functional applications

## 1. Introduction

Thin-film processing plays an increasingly important role in the development of integrated devices because of the current requirements of miniaturization and high integration. Among the several methods used for the fabrication of thin films, chemical solution deposition (CSD) using metal–organic compounds is effective in achieving high homogeneity with low-temperature fabrication, precise control of chemical composition and low equipment costs. Especially in the field of ferroelectrics, the representative ferroelectric materials generally contain an element that easily volatilizes or changes its valence state. Therefore, optimal chemical composition control is indispensable for the fabrication of ferroelectric thin films such as Pb(Zr,Ti)$O_3$-, $Bi_4Ti_3O_{12}$-, (K,Na)$NbO_3$- and $BiFeO_3$-based thin films,[1–7] all of which have been intensively studied for applications in several thin-film electronic devices.

Recently, lead-free ferroelectric thin films have received considerable attention due to environmental issues. Among the numerous lead-free materials, $K_{0.5}Na_{0.5}NbO_3$ (KNN) is a promising candidate, because it has a relatively high Curie temperature and excellent ferroelectric and piezoelectric properties.[8–11] Thus, KNN and KNN-based thin films have been fabricated using several techniques.[4,5,12–25] In the case of CSD-derived thin films, several factors such as the selection of starting materials and the optimization of chemical compositions as well as the processing conditions including the control of the molecular structure of the metal–organic precursor in solution strongly affect the crystallographic phase, microstructures and electrical properties of the resultant thin films. We have previously synthesized perovskite polycrystalline KNN thin films on Pt/$TiO_x$/$SiO_2$/Si substrates by using a metal–organic precursor solution[4,5] and showed that excess amounts (10 mol%) of K and Na are very effective in improving leakage-current properties of the resultant thin films, and enable the evaluation of ferroelectric and piezoelectric properties of the perovskite KNN films.[4] However, the ferroelectric properties of these films were not sufficiently compared with those of lead–zirconate–titanate-based thin films. Thus, further investigations on several processing factors are needed to improve the electrical properties of CSD-derived KNN thin films. Although research and development of CSD-derived KNN-based thin films have been conducted by several researchers,[4,5,15,20,21,23,25] the molecular structure of the KNN precursor in solution has never been reported. Control over

* Corresponding author. Tel.: +81 52 789 2751; fax: +81 52 789 2133.
*E-mail address:* sakamoto@esi.nagoya-u.ac.jp (W. Sakamoto).

0955-2219/$ – see front matter © 2011 Elsevier Ltd. All rights reserved.
doi:10.1016/j.jeurceramsoc.2011.04.031

the crystal orientation growth of thin films associated with the polarization direction is required to maximize the utilization of the properties of perovskite oxides for several applications using ferroelectricity and piezoelectricity. However, the effect of crystal growth orientation on the electrical properties of CSD-derived KNN thin films has not been studied sufficiently.

This paper focuses on the synthesis of highly oriented KNN thin films in perovskite phase by using a structure-optimized complex metal–alkoxide precursor solution. The molecular structure of the KNN precursor in solution was analyzed by nuclear magnetic resonance (NMR) spectroscopy. Furthermore, the orientation growth and electrical properties of the CSD-derived KNN thin films on Pt(1 0 0)/MgO(1 0 0) substrates were also investigated.

## 2. Experimental procedure

$KOC_2H_5$, $NaOC_2H_5$ and $Nb(OC_2H_5)_5$ (Kojundo Chemical, Japan) were selected as starting metal–alkoxide compounds for the preparation of KNN precursor solutions. Since the starting metal alkoxides are extremely sensitive to moisture, 2-methoxyethanol, which was used as a solvent, was dried over molecular sieves and distilled prior to use. Desired amounts of $KOC_2H_5$, $NaOC_2H_5$ and $Nb(OC_2H_5)_5$, corresponding to $K_{0.5}Na_{0.5}NbO_3$ with 10 mol% excess amounts of K and Na, were dissolved in absolute 2-methoxyethanol. In this case, excess K and Na alkoxides were added to compensate for their loss due to their volatility during heating. The mixed solution was then refluxed for 18 h and concentrated to yield a 0.5 mol/l homogeneous solution. The entire procedure was conducted in a dry $N_2$ atmosphere.

The KNN thin films were fabricated using the precursor solution by spin coating on Pt(1 0 0)/MgO(1 0 0) and Pt(1 1 1)/$TiO_x$/$SiO_2$/Si substrates. A Pt(1 0 0) layer was grown on MgO(1 0 0) by radio-frequency (RF) magnetron sputtering at 550 °C in an argon and oxygen gas (1/1) mixture (pressure of 0.5 Pa) referred to the literature.[26] The thickness of the Pt layer in both substrates was approximately 200 nm. Prior to spin coating, the substrates were cleaned by soaking in 2-methoxyethanol. The KNN thin films on Pt(1 0 0)/MgO(1 0 0) substrates were prepared as follows: the deposited precursor films were heat-treated by heating up to 300 °C at a rate of 5 °C/min, then heating at 300 °C for 30 min, followed by subsequent heating up to 650 °C, which was maintained for 10 min. On the other hand, for the preparation of KNN thin films on the Pt(1 1 1)/$TiO_x$/$SiO_2$/Si substrate, the same procedure was followed, except that the heating rate was 10 °C/min. These heat treatments were carried out in an $O_2$ flow and film thicknesses of 600–650 nm were achieved by repeating the coating/heat-treatment cycle.

Furthermore, for fabricating KNN thin films on Pt(1 0 0)/MgO(1 0 0) substrates, a buffer layer was formed on the substrate by using a 0.05 mol/l KNN precursor solution. A thin layer of the KNN precursor on the substrate was heat-treated at 650 °C for 10 min under the same conditions described above and the precursor film was then coated on the precrystallized KNN buffer layer by using 0.5 mol/l solution.

$^1H$ and $^{13}C$ NMR spectra were recorded using an INOVA spectrometer system (Varian) in $C_6D_6$ solution by using tetramethylsilane as the internal standard. The $^{93}Nb$ NMR spectrum of the precursor was recorded at 66.05 MHz (JEOL GX270) in a 2-methoxyethanol solution. Chemical shifts of the $^{93}Nb$ spectrum were calibrated with the standard tetramethylammonium hexachloroniobate $(CH_3)_4N[NbCl_6]$ in $CD_3CN$. The prepared films were characterized by X-ray diffraction (XRD; Rigaku RAD RC) analysis using CuKα radiation with a monochromater. The crystallographic alignment of the KNN films on Pt(1 0 0)/MgO(1 0 0) substrates was examined by XRD using Cu Kα radiation with a two-dimensional (2D) detector (BRUKER D8 DISCOVER/μ-HR). The crystallographic phase of the KNN films was identified by Raman microprobe spectroscopy using a 532.30 nm Ar laser beam (JASCO, NRS-1000, 1 μm, 10 mW). The films on the substrates were observed by scanning electron microscopy (SEM; JEOL JSM-5600). To evaluate the electrical properties of the films, 0.2-mm-diameter Pt top electrodes were deposited by DC sputtering on the films and then annealed at 400 °C for 60 min. The Pt layer of the substrates was used as the bottom electrodes. Ferroelectric properties were evaluated using a ferroelectric test system (Toyo Corp., FCE-1) at 1 kHz and at room temperature and −190 °C in a wafer cryostat (Sanwa Musen WM-363-1) under vacuum (1.0 Pa). The current density (*J*)–electric field (*E*) characteristics of the KNN thin films were measured at room temperature using an electrometer/high-resistance meter (Keithley 6517A): an incremental voltage step of 0.1 V with a duration of 1 s was used and the current was measured at the end of each voltage step.

## 3. Results and discussion

### 3.1. Synthesis and analysis of KNN precursor solution

KNN precursor solutions were prepared from $KOC_2H_5$, $NaOC_2H_5$ and $Nb(OC_2H_5)_5$ in 2-methoxyethanol. These solutions have a sufficient long-term stability. The effect of the 2-methoxyethanol ligand on the KNN precursor was analyzed by $^1H$ and $^{13}C$ spectroscopy. Fig. 1 shows $^1H$ and $^{13}C$ NMR spectra of the KNN precursor. The three signals of the 2-methoxyethoxy groups ($CH_3OCH_2CH_2O$) are observed at 3.2 ppm (singlet, $C\underline{H}_3OCH_2CH_2O$–): 3.6 ppm (triplet, $CH_3OC\underline{H}_2CH_2O$–) and 4.6 ppm (triplet, $CH_3OCH_2C\underline{H}_2O$–) (Fig. 1(a)). The signal corresponding to the hydroxy group (singlet, –O<u>H</u>) at 2.9 ppm disappears compared with the $^1H$ NMR spectrum of 2-methoxyethanol, and the peak at 3.6 ppm (quartet, $CH_3OCH_2C\underline{H}_2O$–H) shifts downfield to 4.6 ppm, which suggests the formation of $CH_3OCH_2CH_2O$–*M* bond (*M*: metal). Fig. 1(b) shows the $^{13}C$ NMR spectrum of KNN precursor. The three signals of the 2-methoxyethoxy groups ($CH_3OCH_2CH_2O$) are observed at 58 ppm ($\underline{C}H_3OCH_2CH_2O$–), 76 ppm ($CH_3O\underline{C}H_2CH_2O$–) and 70 ppm ($CH_3OCH_2\underline{C}H_2O$–). The peak at 62 ppm ($CH_3OCH_2\underline{C}H_2O$–H) of the free 2-methoxyethanol shifts

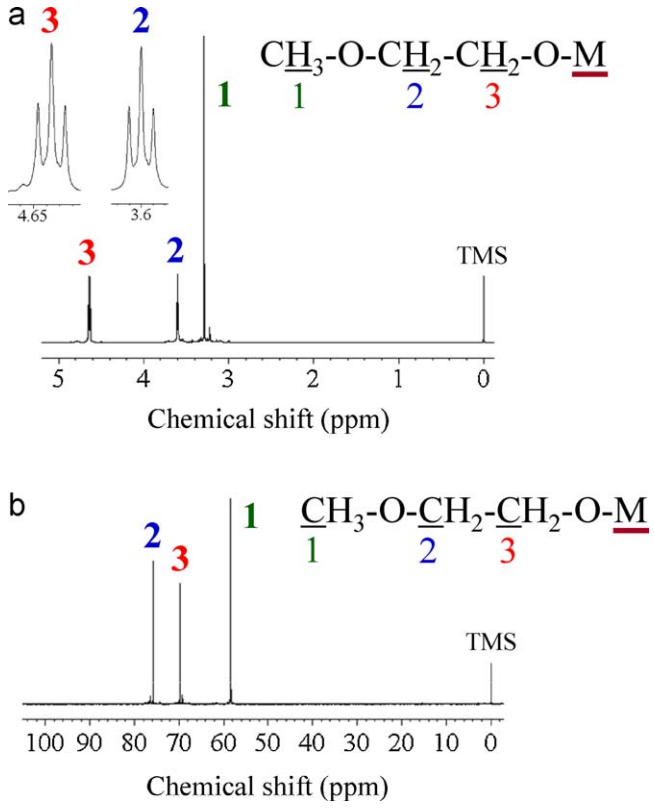


Fig. 1. (a) $^{1}$H NMR and (b) $^{13}$C NMR spectra of KNN precursor (solvent: $C_6D_6$, TMS: tetramethyl silane).

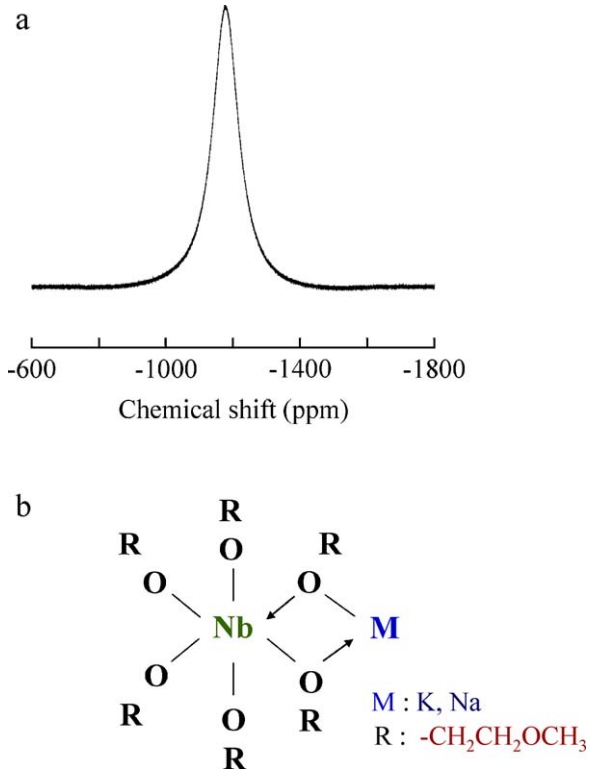


Fig. 2. (a) $^{93}$Nb NMR spectrum of KNN precursor solution (solvent: 2-methixyethanol) and (b) proposed structure of KNN precursor.

downfield to 70 ppm ($CH_3OCH_2\underline{C}H_2O$–*M*). These results indicate that the ethoxy ligands on the metals of the starting materials are entirely substituted by methoxyethoxy groups.

Fig. 2(a) shows the $^{93}$Nb NMR spectrum of the KNN precursor solution. The $^{93}$Nb NMR spectrum of the starting material $Nb(OEt)_5$ exhibits two or three broad signals because of association and ligand exchanges[27] and is remarkably different from that of the KNN precursor solution. $^{93}$Nb NMR of the KNN precursor in 2-methoxyethanol solution shows a single signal at −1178 ppm with a half-width of 5960 Hz. This result indicates the formation of a complex alkoxide comprising highly symmetric niobium–oxygen octahedra of $[Nb(OR)_6]$.[27] The single signal is in good agreement with the structure of $KNb(OEt)_6$ proposed by Mehrotra et al.[28] Since $^{93}$Nb has a quadrupole moment ($I = 9/2$), the broadening of signals is usually observed. The composition of KNN corresponds to a mixture of $0.5K[Nb(OR)_6]$ and $0.5Na[Nb(OR)_6]$. The KNN precursor consists of $MNb(OR)_6$ ($M$ = K, Na, $R = OCH_2CH_2OCH_3$) units, which are mixed at a molecular level in solution. On the basis of the NMR spectroscopic data, the proposed structure of the precursors is shown in Fig. 2(b) and consists of potassium and sodium hexaalkoxy niobates with highly symmetric Nb–O octahedra. Since KNN is the solid solution between $KNbO_3$ and $NaNbO_3$, the tailored complex alkoxides dissolve uniformly at the molecular level in solution and are suitable for the preparation of KNN thin films.

### 3.2. *Crystallization and orientation mechanism of (1 0 0)-oriented KNN thin films*

Crystalline KNN thin films were fabricated by heat treatment of the KNN precursor films on the substrates. Fig. 3 shows the XRD profiles of KNN thin films on Pt(1 0 0)/MgO(1 0 0) and Pt(1 1 1)/$TiO_x$/$SiO_2$/Si substrates and the KNN powder crystallized at 650 °C. The KNN powder sample was prepared by removing the solvent from the precursor solution. The precur-

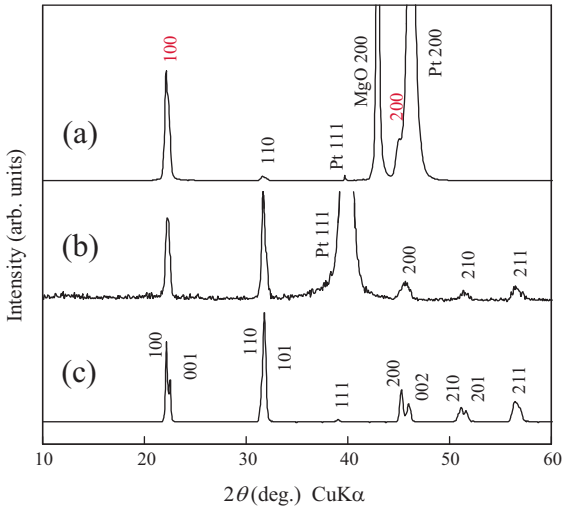


Fig. 3. XRD patterns of KNN thin films prepared at 650 °C on (a) Pt(1 0 0)/MgO(1 0 0) and (b) Pt/$TiO_x$/$SiO_2$/Si substrates and (c) perovskite KNN powder crystallized at 650 °C.

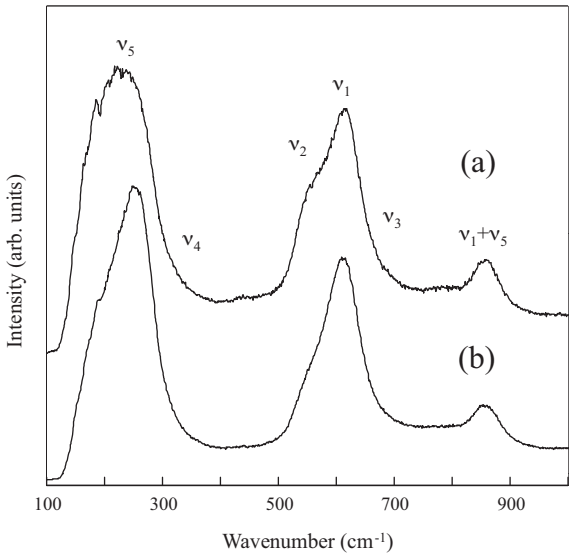


Fig. 4. Raman microprobe spectra of KNN thin films fabricated at 650 °C on (a) Pt(1 0 0)/MgO(1 0 0) and (b) Pt/$TiO_x$/$SiO_2$/Si substrates. The Raman scattering assignments of the internal vibration modes of $NbO_6$ octahedra ($\nu_1$, $\nu_2$, $\nu_3$, $\nu_4$, $\nu_5$, $\nu_1+\nu_5$) are from Kakimoto et al (Ref. 32).

sor powder was heat-treated under the same conditions as the KNN thin films on Pt/$TiO_x$/$SiO_2$/Si to yield crystalline KNN powders. Although the diffraction lines of the crystalline KNN powder were similar to those of tetragonal (or orthorhombic) perovskite oxides, the alkoxy-derived KNN thin films crystallize into the pseudo cubic perovskite phase and there is no secondary phase such as $K_4Nb_6O_{17}$. The XRD patterns of the films on Pt(1 0 0)/MgO(1 0 0) show a strong 1 0 0 reflection accompanied with a small 1 1 0 peak. In Fig. 3(a), the 2 0 0 reflection of KNN is superimposed with Pt(2 0 0). The $d$ value of Pt(2 0 0) is a little smaller than that of KNN(2 0 0). Moreover, the intensity of the 2 0 0 reflection of Pt is much higher than that of the 2 0 0 reflection of KNN. Therefore, in this case, the diffraction line seems to a little widen to lower $2\theta$ angle region. On the other hand, the KNN thin films prepared on Pt(1 1 1)/$TiO_x$/$SiO_2$/Si substrates are polycrystalline with no preferred orientation. The degree of {1 0 0} orientation in the KNN films was evaluated according to the Lodgering equation.[29] From the XRD data in Fig. 3, Lodgering factors of the KNN thin films prepared on Pt(1 0 0)/MgO(1 0 0) and Pt/$TiO_x$/$SiO_2$/Si were calculated to be 95% and 0%, respectively.

For the oriented thin films, it is difficult to judge clearly whether the KNN films on Pt(1 0 0)/MgO(1 0 0) crystallize in the perovskite phase or other phases, since the XRD patterns have only a few peaks. Therefore, KNN thin films on Pt(1 0 0)/MgO(1 0 0) substrates were examined further by Raman microprobe spectroscopy as in the case of tungsten bronze (Sr,Ba)$Nb_2O_6$ and (Pb,Ba)$Nb_2O_6$ thin films.[30,31] Fig. 4 illustrates the Raman spectra of KNN thin films prepared on Pt/MgO(1 0 0) and Pt/$TiO_x$/$SiO_2$/Si substrates. The KNN thin film prepared on the Pt/$TiO_x$/$SiO_2$/Si substrate crystallizes in the polycrystalline perovskite KNN single phase, as shown in Fig. 3(b). From Fig. 4, both the oriented and the polycrystalline KNN films on Pt/MgO(1 0 0) and Pt/$TiO_x$/$SiO_2$/Si substrates display the characteristic Raman scatterings of the internal vibration modes of $NbO_6$ octahedra ($\nu_1$, $\nu_2$, $\nu_3$, $\nu_4$, $\nu_5$, $\nu_1+\nu_5$), which correspond to the stretching modes [$A_{1g}(\nu_1)$, $E_g(\nu_2)$, $F_{1u}(\nu_3)$] and the bending modes [$F_{1u}(\nu_4)$, $F_{2g}(\nu_5)$], as reported by Kakimoto et al.[32] The bending mode of $F_{2u}(\nu_6)$ is not clearly observed in Fig. 4. The profiles in the figure are consistent with those of KNN ceramics in a former report,[32] because no scattering mode of the second phase is observed. Thus, the direct formation of the perovskite KNN phase in synthesized KNN films without an intermediate phase is confirmed.

To investigate the crystallographic alignment of the KNN thin films on Pt(1 0 0)/MgO(1 0 0) substrates, X-ray pole figure measurements are employed. Fig. 5(a) shows the (1 0 1) X-ray pole figure of the KNN layer on Pt(1 0 0)/MgO(1 0 0) substrate, where $\phi$ is the rotation axis perpendicular to the film plane and $\psi$ is the rotation axis perpendicular to $\phi$ and $\theta$. The {1 0 1} planes intersect the ⟨0 0 1⟩ direction of the film at 45° and have a fourfold symmetry around ⟨001⟩. Fig. 5(b) shows that the (2 2 0) X-ray pole figure of the Pt layer on MgO(1 0 0) shows spots every 90° along $\phi$ at $\psi = 45°$. The three-dimensional (3D) relationship between Pt(1 0 0) and MgO(1 0 0) is confirmed by the fourfold symmetry of the pole figure, which indicates that the KNN films are oriented in both the c and a, b directions on the Pt(1 0 0)/MgO(1 0 0) substrate. In the Pt(1 0 0)/MgO(1 0 0) substrate, the a-axis of MgO is consistent with that of Pt, indicating that the crystal lattice plane of KNN is grown with a cube-on-cube relationship on the Pt(1 0 0)/MgO(1 0 0) substrate. This is in agreement with the K(Ta,Nb)$O_3$ thin film growth on Pt(1 0 0)/MgO(1 0 0) substrates prepared by the CSD process.[27]

The formation of the perovskite phase on Pt(1 0 0)/MgO(1 0 0) is attributed to the atomic alignment relationship between KNN(1 0 0) and Pt(1 0 0), as shown in Fig. 5(c). The pseudo cubic phase of KNN has a lattice parameter of 0.3962 nm (measured value from XRD) and the

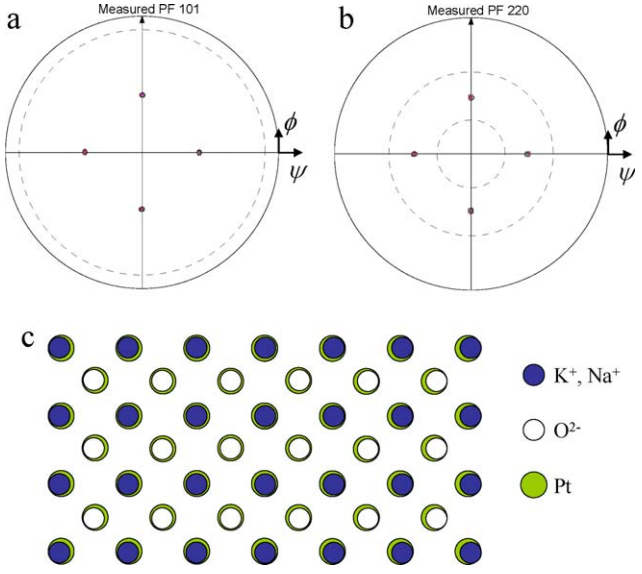


Fig. 5. X-ray pole figures of (a) KNN thin film fabricated at 650 ◦C on Pt(1 0 0)/MgO(1 0 0) measured for (1 0 1) plane, (b) Pt thin film on MgO(1 0 0) measured for (2 2 0) and (c) atomic alignment relationship between KNN(1 0 0) plane and Pt(1 0 0) plane based upon pole figure measurements.

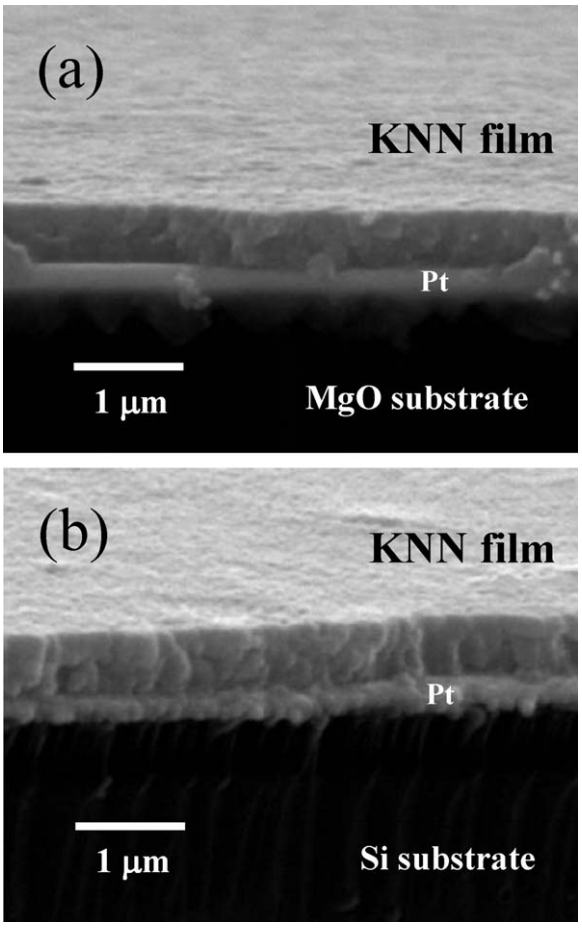


Fig. 6. Cross-sectional SEM images of KNN thin films fabricated at 650 °C on (a) Pt(1 0 0)/MgO(1 0 0) and (b) Pt/$TiO_x$/$SiO_2$/Si substrates.

deposited Pt layers on MgO(1 0 0) have a (1 0 0) orientation with a 3D alignment. Platinum has a face-centered cubic atomic packing with a lattice parameter of 0.3926 nm (measured from XRD). The lattice mismatch between KNN(1 0 0) and Pt(1 0 0) is calculated to be 0.92% on the basis of the pole-figure measurements and their measured lattice parameters. Thus, the crystallization of KNN with both in-pane and out-of-plane orientations results from the crystallographic matching of KNN(1 0 0) to Pt(1 0 0).

Fig. 6 shows the cross-sectional SEM images of KNN thin films prepared at 650 °C on Pt/MgO(1 0 0) and Pt/$TiO_x$/$SiO_2$/Si substrates. These films are crack-free and dense, with a smooth surface and uniform thickness of approximately 650 nm for Pt/MgO(1 0 0) and 600 nm for Pt/$TiO_x$/$SiO_2$/Si. Furthermore, from atomic force microscopy surface images, the root-mean-square roughness values of the KNN thin films prepared on Pt/MgO(1 0 0) and Pt/$TiO_x$/$SiO_2$/Si substrates are 2.3 nm and 2.9 nm, respectively, in a 1 μm × 1 μm area. The film quality is sufficient for the characterization of several electrical properties.

### 3.3. Electrical properties of (1 0 0)-oriented KNN thin films

Fig. 7 shows the *J–E* characteristics (at room temperature) of KNN thin films prepared on Pt/MgO(1 0 0) and Pt/$TiO_x$/$SiO_2$/Si substrates. For the KNN thin films prepared on Pt/MgO(1 0 0), the leakage-current density rapidly increases at 40 kV/cm when the electric field is applied from the bottom electrode to the top electrode [positive electric field in Fig. 7(a)]. The current density of the film changes from the order of $10^{-7}$ A/cm$^2$ at 40 kV/cm to $10^{-4}$ A/cm$^2$ at 80 kV/cm. The most remarkable difference in the KNN thin-film fabrication process is the heating rate in the heat-treated process. With a decrease in heating rate, the total heating time increases; hence, the K and Na ions become volatile, yielding *A*-site ion vacancies. This volatility of K and Na ions triggers the formation of oxygen vacancies to maintain the charge neutrality in the perovskite KNN films. Therefore, cation and anion defects are generated in KNN thin films during the crystallization heat treatment. The distribution of oxygen vacancies originating from compositional fluctuation of K and Na in the film is important for the leakage-current properties. In addition, oxidation of the oxygen vacancies should be considered as reported for KNN single crystals.[33] A relatively high leakage current in the KNN thin films is induced by oxidation, leading to electron–hole ($h^\bullet$) (p-type) conduction, which is expressed as the defect reaction formula ($V_o^{\bullet\bullet} + 1/2O_2 \rightarrow O_o^\times + 2h^\bullet$). In this formula, $V_o^{\bullet\bullet}$ indicates the vacancy at the oxide-ion site $O_o^\times$ and represents $O^{2-}$ at the oxide-ion site. In particular, the segregation of oxygen vacancies near the interface between the top electrode and the KNN thin film may affect the electrode/KNN contact, leading to asymmetric *J–E* properties, as shown in Fig. 7(a). Similar *J–E* curve behaviors have been reported for the KNN thin film.[5]

The leakage-current density of the KNN thin films crystallized on Pt/$TiO_x$/$SiO_2$/Si substrate is almost constant, from about $10^{-7}$ A/cm$^2$ up to an applied field of 90 kV/cm, and then increases to $10^{-5}$ A/cm$^2$ at 150 kV/cm [Fig. 7(b)]. The appropriate heating rate enables the optimization of the number of *A*-site ions volatilized during the heat treatment in which the formation of *A*-site ion vacancies are suppressed with oxygen vacancies, even when the KNN thin films are crystallized at 650 °C. In this study, to obtain highly oriented KNN thin films, a rela-

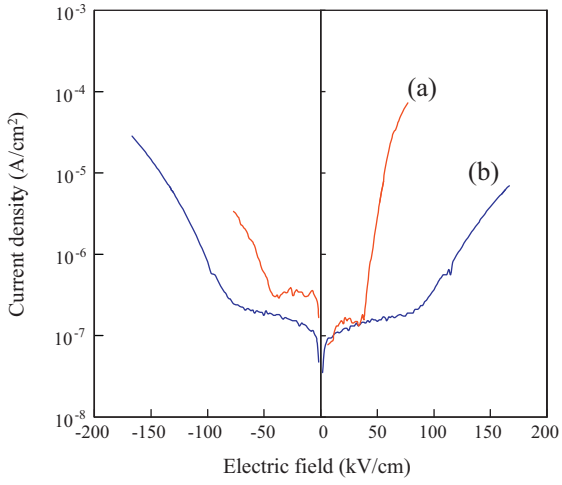


Fig. 7. Leakage-current properties of KNN thin films fabricated at 650 °C on (a) Pt(1 0 0)/MgO(1 0 0) and (b) Pt/$TiO_x$/$SiO_2$/Si substrates. Measurements were performed at room temperature using a ramping-up voltage step of 0.1 V (duration: 1 s) and the current was measured at the end of each voltage step.

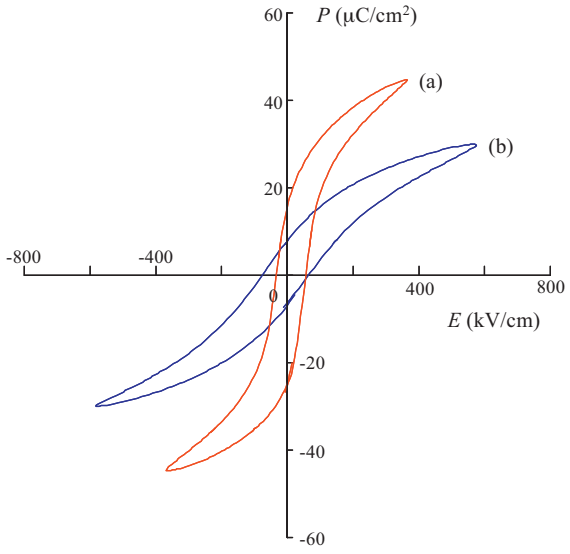


Fig. 8. *P–E* hysteresis loops of KNN thin films fabricated at 650 °C on (a) Pt(1 0 0)/MgO(1 0 0) and (b) Pt/$TiO_x$/$SiO_2$/Si substrates [measured at 1 kHz (−190 °C), film thickness: 600-650 nm].

tively slow heating rate of 5 °C/min is adopted. Improvement of leakage-current properties should be achieved by controlling the defect concentration of K and Na in the film. In addition, further investigations of detailed leakage-current behavior are needed to clarify the mechanisms for achieving sufficient efficiency for practical use.

Fig. 8 shows *P–E* hysteresis loops of KNN thin films prepared on Pt/MgO(1 0 0) and Pt/$TiO_x$/$SiO_2$/Si substrates. These loops were measured at 1 kHz and −190 °C. At room temperature, KNN thin films prepared on Pt/MgO(1 0 0) show poor ferroelectric properties. Higher electric fields could not be applied to the KNN thin films because of the poor leakage-current properties, as shown in Fig. 7. On the other hand, the KNN thin films crystallized on Pt/$TiO_x$/$SiO_2$/Si show typical *P–E* ferroelectric hysteresis loops with a $2P_r$ value of 14 μC/cm$^2$, although the *P–E* hysteresis loops contain slight leakage components. The ferroelectric properties of the KNN thin films prepared on Pt(1 0 0)/MgO(1 0 0) are inferior to those of the KNN thin films prepared on Pt/$TiO_x$/$SiO_2$/Si at room temperature, as the defect structure in the KNN thin films becomes complicated when the KNN thin films are annealed at a slow heating rate over a longer time. To evaluate the potential ferroelectric properties, measurement at low temperature (−190 °C) was carried out and the results are shown in Fig. 8. All the films show well-shaped *P–E* hysteresis loops, which contain little leakage at −190 °C. The KNN thin films prepared on Pt/MgO(1 0 0) Exhibit $2P_r$ and $2E_c$ values of 41 μC/cm$^2$ and 90 kV/cm, respectively, at an applied field around 400 kV/cm. The $P_r$ is larger than those of the reported KNN thin films fabricated by pulsed laser deposition.[12,13] The $2P_r$ values improve by controlling the film orientation; the KNN films with no preferred orientation on Pt/$TiO_x$/$SiO_2$/Si showed $2P_r$ at around 18.0 μC/cm$^2$, as shown in Fig. 8(b). Furthermore, in comparison with other representative lead-free CSD-derived thin films such as $Bi_4Ti_3O_{12}$-,[2,3] $CaBi_4Ti_4O_{15}$-,[34,35] $K_{0.5}Na_{0.5}NbO_3$-[20,21,23,25] and $Bi_{0.5}Na_{0.5}TiO_3$-based thin films,[36,37] the (1 0 0)-oriented KNN thin film possesses higher or comparable $2P_r$ with lower $2E_c$. The imprint behavior of the hysteresis curve, observed for the KNN film on Pr/MgO(1 0 0) in Fig. 8(a), is due to the internal bias caused by the defect formation differences in the film thickness direction during heat treatment (the defect concentration increases around the film surface). Although the relationship between the orientation degree and the properties of the resultant KNN thin films is confirmed in this study, further optimization of the synthesis conditions, particularly more precise control of the K and Na composition in KNN thin films, is required to improve the electrical properties at ambient temperatures. Such thin film synthesis optimization provides the KNN thin films whose piezoelectric and ferroelectric (including fatigue endurance) properties can be characterized, and this study is currently in progress.

## 4. Conclusions

Highly oriented perovskite KNN single-phase thin films were fabricated by CSD using Pt(1 0 0)/MgO(1 0 0) substrates. From NMR data, the KNN precursor consists of $KNb(OCH_2CH_2OCH_3)_6$ and $NaNb(OCH_2CH_2OCH_3)_6$ units, which are mixed at a molecular level in solution. The crystallographic phase of the (1 0 0)-oriented KNN thin film was confirmed by Raman spectroscopic analysis. The 3D relationship between the KNN thin film and Pt(1 0 0)/MgO(1 0 0) substrate was examined by X-ray pole figure measurements. The oriented KNN thin films were grown with a cube-on-cube relationship on the Pt(1 0 0)/MgO(1 0 0) substrates. Although the insulating resistance of the films was not sufficiently high at room temperature, the oriented KNN thin films showed larger ferroelectric polarizations than those with no preferred orientation at relatively low applied electric fields. The oriented KNN thin films prepared at 650 °C showed a ferroelectric *P–E* hysteresis loop with a $2P_r$ value of 41.0 μC/cm$^2$ at −190 °C. Although further improvement in the ferroelectric properties at ambient temperature is still needed, the orientation-controlled KNN thin films developed by CSD in this study show potential for use in lead-free ferroelectric thin-film device applications.

## Acknowledgements

This study was partly supported by the Tatematsu Foundation. The authors are grateful to Dr. Hitoshi Morioka and Dr. Keisuke Saito (Bruker AXS) for their support in the pole figure measurements.

## References

1. Hirano S, Yogo T, Kikuta K, Araki Y, Saitoh M, Ogasawara S. Synthesis of highly oriented lead zirconate lead titanate film using metalloorganics. *J Am Ceram Soc* 1992;**75**:2785–9.
2. Hayashi T, Togawa D, Yamada M, Sakamoto W, Hirano S. Preparation and properties of $Bi_{4-x}La_xTi_3O_{12}$ ferroelectric thin films using excimer UV irradiation. *Jpn J Appl Phys* 2002;**41**:6814–9.

3. Yamada M, Iizawa N, Yamaguchi T, Sakamoto W, Kikuta K, Yogo T, et al. Processing and properties of rare earth ion-doped bismuth titanate thin films by chemical solution deposition method. *Jpn J Appl Phys* 2003;**42**:5222–6.
4. Nakashima Y, Sakamoto W, Maiwa H, Shimura T, Yogo T. Lead-free piezoelectric (K,Na)$NbO_3$ thin films derived from metal alkoxide precursors. *Jpn J Appl Phys* 2007;**46**:L311–3.
5. Nakashima Y, Sakamoto W, Shimura T, Yogo T. Chemical processing and characterization of ferroelectric (K,Na)$NbO_3$ thin films. *Jpn J Appl Phys* 2007;**46**:6971–5.
6. Sakamoto W, Iwata A, Yogo T. Ferroelectric properties of chemically synthesized perovskite $BiFeO_3$–$PbTiO_3$ thin films. *J Appl Phys* 2008;**104**:104106.
7. Sakamoto W, Iwata A, Moriya M, Yogo T. Electrical and magnetic properties of Mn-doped $0.7BiFeO_3$–$0.3PbTiO_3$ thin films prepared under various heating atmospheres. *Mater Chem Phys* 2009;**116**:536–41.
8. Jeager RE, Egerton L. Hot pressing of potassium-sodium niobate. *J Am Ceram Soc* 1962;**45**:208–13.
9. Saito Y, Takao H, Tani T, Nonoyama T, Takatori K, Hommma T, et al. Lead-free piezoceramics. *Nature* 2004;**432**:84–7.
10. Guo Y, Kakimoto K, Ohsato H. Phase transitional behavior and piezoelectric properties of $(Na_{0.5}K_{0.5})NbO_3$–$LiNbO_3$ ceramics. *Appl Phys Lett* 2004;**85**:4121–3.
11. Matsubara M, Yamaguchi T, Sakamoto W, Kikuta K, Yogo T, Hirano S. Processing and piezoelectric properties of lead-free (K,Na)$(Nb,Ta)O_3$ ceramics. *J Am Ceram Soc* 2005;**88**:1190–6.
12. Cho C-R, Grishin A. Self-assembling ferroelectric $Na_{0.5}K_{0.5}NbO_3$ thin films by pulsed laser deposition. *Appl Phys Lett* 1999;**75**: 268–70.
13. Cho C-R, Grishin A. Background oxygen effects on pulsed laser deposited $Na_{0.5}K_{0.5}NbO_3$ films: From superparaelectric state to ferroelectricity. *J Appl Phys* 2000;**87**:4439–48.
14. Cho C-R. c-Axis oriented (Na,K)$NbO_3$ thin films on Si substrates using metalorganic chemical vapor deposition. *Mater Lett* 2002;**57**:781–6.
15. Söderlind F, Käll PO, Helmersson U. Sol–gel synthesis and characterization of $Na_{0.5}K_{0.5}NbO_3$ thin films. *J Cryst Growth* 2005;**281**:468–74.
16. Saito T, Adachi H, Wada T. Pulsed laser deposition of ferroelectric $(Na_{0.5}K_{0.5})NbO_3$-based thin films. *Jpn J Appl Phys* 2005;**44**:573–5.
17. Oh SW, Akedo J, Park JH, Kawakami Y. Fabrication and evaluation of lead-free piezoelectric ceramics LF4 thin film deposited by aerosol deposition method. *Jpn J Appl Phys* 2006;**45**:7465–70.
18. Ryu J, Choi J-J, Hahn B-D, Park D-S, Yoon W-H, Kim K-H. Fabrication and ferroelectric properties of highly dense lead-free piezoelectric $(K_{0.5}Na_{0.5})NbO_3$ thick films by aerosol deposition. *Appl Phys Lett* 2007;**90**:152901.
19. Kanno I, Mino T, Kuwajima S, Suzuki T, Kotera H, Wasa K. Piezoelectric properties of (K,Na)$NbO_3$ thin films deposited on (0 0 1)$SrRuO_3$/Pt/MgO substrates. *IEEE Trans Ultrason Ferroelectr Freq Control* 2007;**54**: 2562–6.
20. Tanaka K, Hayashi H, Kakimoto K, Ohsato H, Iijima T. Effect of (Na,K)-excess precursor solutions on alkoxy-derived (Na,K)$NbO_3$ powders and thin films. *Jpn J Appl Phys* 2007;**46**:6964–70.
21. Wang L, Yao K, Ren W. Piezoelectric $K_{0.5}Na_{0.5}NbO_3$ thick films derived from polyvinylpyrrolidone-modified chemical solution deposition. *Appl Phys Lett* 2008;**93**:092903.
22. Shibata K, Oka F, Ohishi A, Mishima T, Kanno I. Piezoelectric properties of (K,Na)$NbO_3$ films deposited by RF magnetron sputtering. *Appl Phys Express* 2008;**1**:011501.
23. Ahn CW, Jeong ED, Lee SY, Lee HJ, Kang SH, Kim IW. Enhanced ferroelectric properties of $LiNbO_3$ substituted $Na_{0.5}K_{0.5}NbO_3$ lead-free thin films grown by chemical solution deposition. *Appl Phys Lett* 2008;**93**:212905.
24. Abazari M, Akdoğan EK, Safari A. Dielectric and ferroelectric properties of strain-relieved epitaxial lead-free KNN-LT-LS ferroelectric thin films on $SrTiO_3$ substrates. *J Appl Phys* 2008;**103**:104106.
25. Lai F, Li J-F, Zhu Z-X, Xu Y. Influence of Li content on electrical properties of highly piezoelectric (Li,K,Na)$NbO_3$ thin films prepared by sol–gel processing. *J Appl Phys* 2009;**106**:064101.
26. Iijima K, Takayama R, Tomita Y, Ueda I. Epitaxial growth and pyroelectric properties of lanthanum-modified lead titanate thin films. *J Appl Phys* 1986;**60**:2914–9.
27. Yogo T, Kikuta K, Ito Y, Hirano S. Synthesis of highly oriented K(Ta,Nb)$O_3$ (Ta:Nb = 65:35) film using metal alkoxides. *J Am Ceram Soc* 1995;**78**:2175–9.
28. Mehrotra RC, Agrawal MM, Kapoor PN. Alkali-metal hexaalkoxides of niobium and tantalum. *J Chem Soc A* 1968:2673–6.
29. Lotgering FK. Topotactical reactions with ferrimagnetic oxides having hexagonal crystal structures—I. *J Inorg Nucl Chem* 1959;**9**:113–23.
30. Sakamoto W, Yogo T, Kikuta K, Ogiso K, Kawase A, Hirano S. Synthesis of strontium barium niobate thin films through metal alkoxide. *J Am Ceram Soc* 1996;**79**:2283–8.
31. Sakamoto W, Kosugi K, Arimoto T, Yogo T, Hirano S. Chemical processing of potassium substituted $(Pb_{0.6}Ba_{0.4})Nb_2O_6$ powders and thin films through metallo-organics. *J Sol–Gel Sci Technol* 1999;**16**:65–75.
32. Kakimoto K, Akao K, Guo Y, Ohsato H. Raman scattering study of piezoelectric $(Na_{0.5}K_{0.5})NbO_3$-$LiNbO_3$ ceramics. *Jpn J Appl Phys* 2005;**44**:7064–7.
33. Kizaki Y, Noguchi Y, Miyayama M. Defect control for low leakage current in $K_{0.5}Na_{0.5}NbO_3$ single crystals. *Appl Phys Lett* 2006;**89**:142910.
34. Kato K, Fu D, Suzuki K, Tanaka K, Nishizawa K, Miki T. Ferro- and piezoelectric properties of polar-axis-oriented $CaBi_4Ti_4O_{15}$ films. *Appl Phys Lett* 2004;**84**:3771–3.
35. Simões AZ, Ramírez MA, Ries A, Varela JA, Longo E, Ramesh R. Electromechanical properties of calcium bismuth titanate films: a potential candidate for lead-free thin-film piezoelectrics. *Appl Phys Lett* 2006;**88**:072916.
36. Zhang DZ, Zheng XJ, Feng X, Zhang T, Sun J, Dai SH, et al. Ferro-piezoelectric properties of $0.94(Na_{0.5}Bi_{0.5})TiO_3$–$0.06BaTiO_3$ thin film prepared by metal–organic decomposition. *J Alloys Compd* 2010;**504**:129–33.
37. Yu T, Kwok KW, Chan HLW. Preparation and properties of sol–gel-derived $Bi_{0.5}Na_{0.5}TiO_3$ lead-free ferroelectric thin film. *Thin Solid Films* 2007;**515**:3563–6.